Constraining models of initial conditions with elliptic and triangular flow data

Ekaterina Retinskaya, Matthew Luzum, Jean-Yves Ollitrault

Constraining models of initial conditions with elliptic and triangular flow data

Ekaterina Retinskaya,[1] Matthew Luzum,[2,3] and Jean-Yves Ollitrault[4]

[1] *CEA, IPhT, Institut de physique théorique de Saclay, F-91191 Gif-sur-Yvette, France*
[2] *McGill University, 3600 University Street, Montreal QC H3A 2TS, Canada*
[3] *Lawrence Berkeley National Laboratory, Berkeley, CA 94720, USA*
[4] *CNRS, URA2306, IPhT, Institut de physique théorique de Saclay, F-91191 Gif-sur-Yvette, France*

(Dated: January 10, 2014)

We carry out a combined analysis of elliptic and triangular flow data using viscous relativistic hydrodynamics. We show that these data allow to put tight constraints on models of the early dynamics of a nucleus-nucleus collision. Specifically, the rms values of the initial ellipticity ε_2 and the initial triangularity ε_3 are constrained to lie within a narrow band for each centrality. We use these constraints as a filter for existing Monte-Carlo models of initial state, and provide a simple test that can be performed on any candidate model to determine its compatibility with data.

I. INTRODUCTION

Anisotropic flow [1] in heavy-ion collisions is understood as the hydrodynamic response [2] of the strongly-interacting medium to a spatial anisotropy created in the early stages of the collision. Elliptic flow, v_2 [3, 4], originates from the almond shape of the overlap area between the colliding nuclei [5]. Similarly, triangular flow, v_3, is generated by fluctuations of the initial density profile which have a triangular shape [6].

It has long been recognized that the extraction of transport coefficients of the strongly-coupled quark-gluon plasma (in particular, its viscosity over entropy density ratio η/s [7]) from elliptic flow data is hindered by the poor knowledge of the initial geometry [8]. Specifically, different models of the initial state, supplemented with viscous hydrodynamic evolution, can be made compatible with experimental elliptic flow data at the expense of tuning η/s. More recently, a large number of new flow observables have been measured, which can add extra non-trivial constraints. For example, it was noticed that, while either elliptic flow or triangular flow data could be reasonably fit individually by tuning the viscosity in a hydrodynamic calculation, only some models of the initial state could be made compatible with both. Thus, some models can actually be ruled out [9, 10].

The goal of this paper is to propose a systematic approach for constraining models of initial conditions using anisotropic flow data. Early work in this direction was done by the ALICE collaboration, who was able to place constraints on the relative centrality dependence of the initial eccentricity for very central collisions at the LHC, without having to perform hydrodynamic calculations [11]. Here, by combining hydrodynamic simulations with data from Au-Au collisions at $\sqrt{s_{NN}} = 0.2$ TeV [10] and Pb-Pb collisions at $\sqrt{s_{NN}} = 2.76$ TeV [11], we are able to place strong constraints at all centralities. We then use these constraints as a filter for existing models of initial conditions, and we provide a simple test that can be applied to any future model to quickly and easily determine whether it is compatible with these data.

II. METHODOLOGY

The observable we choose for this study is the integrated [12] anisotropic flow v_n, i.e., averaged over the particle transverse momentum. The reason is twofold: First, hydrodynamics is meant to describe the bulk features of particle production, therefore its most robust predictions are for bulk observables. Second, differential anisotropic flow (i.e., its relative dependence on transverse momentum) does not depend much on the initial state[1]: predictions of ideal (non-viscous) hydrodynamics for the differential v_n are to some extent universal [9, 15], while viscous corrections are determined by the late stages of the collision [16, 17]. Therefore one does not lose essential information on the initial state by considering only the integrated anisotropic flow.

We only use two out of the six Fourier harmonics which have been measured [18], namely v_2 and v_3. Again, the reason is twofold: first, they are the largest harmonics for all centralities, hence they are determined with better accuracy. Second, in these two harmonics, the hydrodynamic response to the initial state is dominated by simple linear response [19]. Specifically, elliptic flow v_2 in hydrodynamics is to a good approximation [20] proportional to the participant ellipticity ε_2 [21] and triangular flow is proportional [22] to the participant triangularity ε_3 [6]. ε_n with $n > 1$ is generally defined as [2, 23]

$$\varepsilon_n \equiv \frac{|\int r^n e^{in\phi} \epsilon(r,\phi) r \mathrm{d}r \mathrm{d}\phi|}{\int r^n \epsilon(r,\phi) r \mathrm{d}r \mathrm{d}\phi}, \tag{1}$$

where integration is over the transverse plane in polar coordinates, and $\epsilon(r,\phi)$ denotes the energy density at $z \sim 0$. The system is centered, so that $\int r e^{i\phi} \epsilon(r,\phi) r \mathrm{d}r \mathrm{d}\phi = 0$.

Linear response is also a reasonable approximation for v_1 [24], with a specific definition of the dipole asymmetry ε_1 [2]. The constraints on the initial state from v_1

[1] except at high transverse momentum where a granular density profile yields less anisotropic flow [13] than a smooth density profile. This effect [14] could be used to study such additional features of the initial state, but we will see that those features do not affect the conclusions in this work.

were studied in a previous publication [25]. Higher order Fourier harmonics of anisotropic flow (v_4, v_5, v_6) have a more complicated relation to initial-state properties because of large nonlinear terms in the hydrodynamic response [15, 26–28].

The linear-response approximation states

$$v_n = \left(\frac{v_n}{\varepsilon_n}\right)_h \varepsilon_n, \tag{2}$$

with $n = 2, 3$, where v_n on the left-hand side is the measured flow in a given collision event. The first factor on the right-hand side is the hydrodynamic response to the initial anisotropy [2, 9], which is assumed independent of the initial profile for a given centrality, while the second factor depends only on the initial state and encodes all information about event-by-event fluctuations. Experimental data for moments of the event-by-event v_2 and v_3 distribution, combined with hydrodynamical calculations of $(v_2/\varepsilon_2)_h$ and $(v_3/\varepsilon_3)_h$, thus yield the values of the same moments of the initial anisotropies ε_2 and ε_3. Here, we use ALICE data inferred from two-particle correlations [11] and PHENIX data which use an event-plane method [10]. In practice, both methods yield the root-mean-square (rms) value of the event-by-event distribution of v_n [29].[2] Eq. (2) gives:

$$\sqrt{\langle v_n \rangle^2} = \left(\frac{v_n}{\varepsilon_n}\right)_h \sqrt{\langle \varepsilon_n \rangle^2}\ . \tag{3}$$

Therefore the constraints we obtain on ε_n also relate to rms values.

There are several sources of uncertainties in the hydrodynamic response: once these uncertainties are taken into account, the predictions span some region in the (rms ε_3, rms ε_2) plane. As we show in Sec. III, this region turns out to be a narrow band. This puts strong constraints on existing models of initial conditions, which are scrutinized in Sec. IV.

III. UNCERTAINTIES IN THE RESPONSE

Hydrodynamical modeling [32] consists of three stages. It first uses as input an initial condition for the energy-momentum tensor of the system at an early stage of the collision, which is provided by some model of the early dynamics. Second, one evolves this initial condition through the equations of relativistic hydrodynamics. Finally, the fluid is converted into hadrons. Every step of this calculation comes with its own uncertainties. Investigating sources of uncertainty [33] in hydrodynamic modeling requires to carry out a large number of numerical calculations, and the computational effort of a state-of-the-art calculation can become prohibitively expensive [34]. This cost can be reduced by orders of magnitude at the expense of a few simplifying assumptions. For each of the three stages, we now describe the simplifications which can be made, and identify the leading source of uncertainty.

1. Initial conditions: our calculation uses boost-invariant initial conditions [35]. This amounts to neglecting the rapidity dependence of correlations due to anisotropic flow, which is known to be small at LHC energies [18, 36] but may be larger at RHIC [37]. In order to compute the hydrodynamic response in the second harmonic, $(v_2/\varepsilon_2)_h$, we parameterize the transverse density with an optical Glauber model, with an impact parameter that corresponds to the rms impact parameter of each bin in a Monte Carlo Glauber calculation. The overall normalization is then set to match the observed charged multiplicity [38, 39]. In a centered polar coordinate system (r, ϕ), the optical Glauber profile has $\phi \to \phi + \pi$ symmetry for a symmetric collision, hence $\varepsilon_3 = v_3 = 0$. In order to compute the response v_3/ε_3, we introduce by hand a triangularity by deforming the optical Glauber profile as follows [9]:

$$\epsilon(r, \phi) \to \epsilon\left(r\sqrt{1 + \varepsilon_3' \cos(3(\phi - \Phi_3))}, \phi\right), \tag{4}$$

where ε_3' is magnitude of the deformation, and Φ_3 its orientation. The nonlinear coupling between v_2 and v_3 [27] induces a small modulation of v_3 with Φ_3, whose relative magnitude scales like $(\varepsilon_2)^3 \cos(6\Phi_3)$ (the reaction plane is chosen along the x axis). We find this dependence to be 1% or less in all cases: therefore we neglect it and choose $\Phi_3 = 0$ for all calculations. We have also checked that the dependence of the ratio $(v_3/\varepsilon_3)_h$ on the values chosen for ε_3' [9] is negligible. This calculation uses the same values of ε_3' as [9]. Note that recentering the distribution after deformation shifts the center by a distance proportional to $\varepsilon_2\varepsilon_3$. This in turn results in a decrease of ε_3 of relative order $(\varepsilon_2)^2$. This recentering correction was neglected in [9] and the hydrodynamic response was therefore underestimated by up to 10% for peripheral collisions.

Within our linear-response approximation (2), the hydrodynamic response $(v_n/\varepsilon_n)_h$ is assumed independent of the fine structure of the initial profile. Event-by-event ideal hydrodynamic calculations [40] have proven that a such a "single-shot" calculation with smooth initial condition yields the same value of $(v_n/\varepsilon_n)_h$, within a few %, as a calculation with fluctuating initial conditions averaged over many events, while event-by-event viscous hydrodynamic calculations show an even stronger correlation between initial anisotropy ε_n and v_n [19].

In order to estimate quantitatively the dependence of $(v_n/\varepsilon_n)_h$ over the initial profile, we use two different definitions of ε_n, weighted either with energy density (as in Eq. (1)) or with entropy density. Both weightings yield approximately equally good predictors of v_n [26]. So any difference in prediction from one weighting versus

[2] The event-plane method gives a result which coincides with the rms value in the limit of low resolution [30], and the PHENIX analysis has a low resolution [31].

the other is an indication of the size of the uncertainty due to the linear approximation. For central collisions, the particular deformation that we choose to create triangular flow, Eq. (4), gives the exactly same value of ε_3 irrespective of whether one weights with entropy or energy [9]: therefore our calculation is unable to tell the difference between the two. However, values of ε_2 differ for the optical Glauber model, and we use the resulting difference in $(v_2/\varepsilon_2)_h$ as part of our error bar.

The thermalization time t_0, at which hydrodynamics becomes a good approximation [41], is poorly constrained. Early calculations [42] used to neglect transverse flow for $t \leq t_0$ (where t_0 is typically of order 1 fm/c). However, the transverse expansion starts immediately after the collision, whether or not the system thermalizes. This "initial flow" has proven essential in understanding interferometry data [43–45]. Furthermore, it is to some extent universal [46] and can be obtained simply, in a traditional calculation with vanishing flow at t_0, by letting t_0 go to unrealistically small values [44]. In order to estimate the uncertainty due to initial flow, we run two sets of calculations with $t_0 = 0.5$ fm/c and $t_0 = 1$ fm/c: linearity of initial transverse flow at early times [47] can then be used to extrapolate to smaller values.

2. Fluid expansion: The main source of uncertainty in the hydrodynamic evolution itself is the value of the shear viscosity of the strongly-interacting quark-gluon plasma, which is poorly constrained so far, either from theory [48] or experiment [33, 49]. We take this uncertainty into account by varying η/s from 0 to 0.24 in steps of 0.04. If η/s is too large, hydrodynamics itself breaks down [50]. Effects of bulk viscosity [16, 51] on the integrated flow are smaller [52], even though the bulk viscosity may be large for some values of the temperature [53]. Second-order corrections [54] have a negligible effect [8].

3. Hadronic stage: Eventually, the fluid expands and can be described as a gas of hadrons with collective and thermal motion. An open question in the description of the hadronic phase is to what extent hydrodynamics is a valid approach. Instead, a common approach at RHIC energies was to couple hydrodynamics to a hadronic "afterburner" simulating hadronic decays and two-body collisions [55–57]. Although these afterburners usually have little affect on integrated properties of unidentified hadrons, this approach has proven useful for reproducing the elliptic flow and momentum spectra of identified particles. Hadronic afterburners are also being implemented at LHC energies [58, 59]. Besides, it has been pointed out that hydrodynamics with bulk viscosity in the hadronic phase [60] also succeeds in reproducing identified particle properties [61].

In this paper, we assume for simplicity that hydrodynamics still applies in the hadronic phase, with a single freeze-out temperature [42]. When changing the initial time in the hydrodynamic calculation, we tune the freeze-out temperature in such a way that the average transverse momentum of charged particles $\langle p_T \rangle$ is unchanged: smaller values of t_0 thus imply larger freeze-out temperatures. We neglect hadronic collisions below freeze-out, but resonance decays are taken into account.

In viscous hydrodynamics, a significant source of uncertainty is the momentum distribution at freeze-out, which deviates from a thermal distribution due to the viscous correction [62, 63]. The momentum dependence of this viscous correction involves microscopic information about hadronic cross-sections [64]. The quadratic ansatz [62] is the most commonly used. However, a linear ansatz gives better agreement with v_4 data [65]. In order to estimate the uncertainty associated with the modeling of freeze-out, we perform two sets of calculations with the linear and quadratic ansatz.

The code we use to solve hydrodynamics is the same as in Ref. [38], with resonance decays taken into account after freeze-out.

We compute v_2 and v_3 for outgoing hadrons using similar experimental cuts as the experimental data that we compare to. Specifically, the ALICE Collaboration [11] analyzes v_n for all charged hadrons in transverse momentum range $0.2 < p_t < 5$ GeV/c and pseudorapidity range $|\eta| < 0.8$. The PHENIX Collaboration [10] uses the cuts $0.25 < p_t < 4$ GeV/c and $|\eta| < 0.35$. Since our model has longitudinal boost invariance, our results are independent of rapidity. Because of the difference in rapidity and pseudorapidity, however, the cut in η must be taken into account in a precision calculation [66]. It typically increases v_2 by 3% and v_3 by 4%.

An additional subtlety of the ALICE analysis is that the method uses pair correlations, with a pseudorapidity gap $|\Delta\eta| > 1$ between particles in the pair in order to suppress nonflow correlations [67]. The analysis thus excludes particles at $|\eta| < 0.2$, and gives more weight to particles near the boundary $|\eta| = 0.8$, since all *pairs* are weighted identically. We also take into account this additional cut in $\Delta\eta$, which typically decreases v_2 by 0.3% and v_3 by 0.4%.

Fig. 1 illustrates the effects of several sources of uncertainty on the root-mean-square values of $(\varepsilon_2, \varepsilon_3)$ extracted from Eq. (3) (for the 5% most central Pb-Pb collisions at the LHC). Each point represents a hydrodynamic calculation with different parameters. As the viscosity increases, the hydrodynamic response $(v_n/\varepsilon_n)_h$ decreases, therefore the rms ε_n increases. The lines drawn in the $(\varepsilon_3, \varepsilon_2)$ plane as η/s varies are well fitted by a power law:

$$\sqrt{\langle \varepsilon_2^2 \rangle} = C \left(\sqrt{\langle \varepsilon_3^2 \rangle} \right)^k , \tag{5}$$

where $k = 0.6$, and C is fixed. k is the ratio of the relative change in v_2 to the relative change in v_3 when η/s increases. The fact that $k < 1$ expresses that viscosity has a smaller effect on v_2 than on v_3.

Other sources of uncertainty in the hydrodynamic prediction result in uncertainties in the coefficient C in Eq. (5). Switching from the quadratic to the linear freeze-out ansatz has a very small effect, which is visible only for the largest values of η/s. Adding initial flow by starting the evolution earlier, at $t_0 = 0.5$ fm/c, yields more

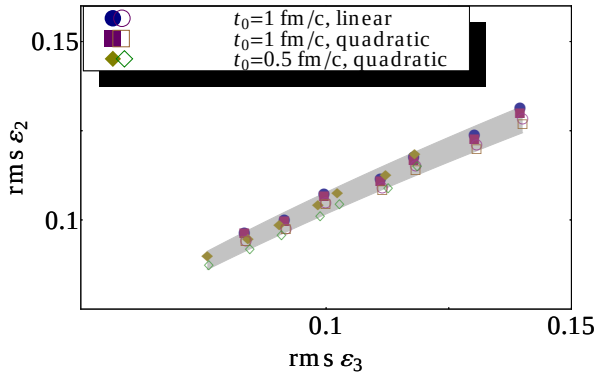

FIG. 1. (Color online) Root-mean-square values of $(\varepsilon_2, \varepsilon_3)$ implied by hydrodynamic calculations in combination with ALICE data for the 5% most central Pb-Pb collisions at $\sqrt{s_{NN}} = 2.76$ TeV. Squares: $t_0 = 1$ fm/c with quadratic freezeout. Circles: $t_0 = 1$ fm/c with linear freezeout. Diamonds: $t_0 = 0.5$ fm/c with quadratic freezeout. Closed symbols correspond to energy density weighting, open symbols to entropy density weighting. For each symbol type, the 7 points correspond to different values of η/s, from 0 to 0.24 (from left to right) in steps of 0.04. The shaded band is the area between two curves of the type (5) with $C = C_{\rm min}$ and $C = C_{\rm max}$, where the values of $C_{\rm min}$ and $C_{\rm max}$ are chosen such that all hydro points lie within the band.

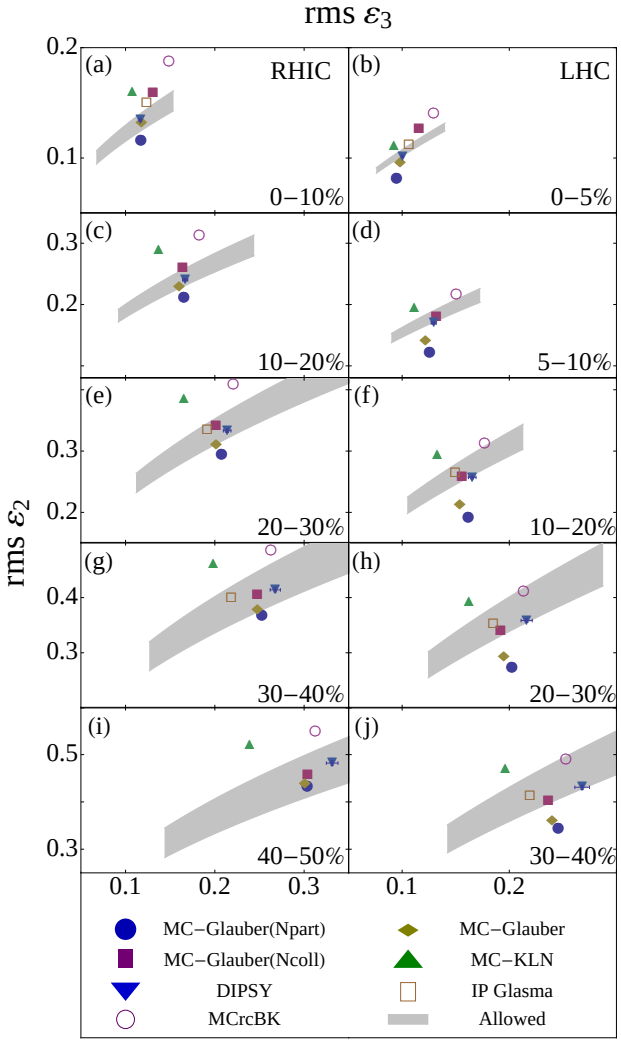

FIG. 2. (Color online) Shaded bands are root-mean-square values of $(\varepsilon_2, \varepsilon_3)$ allowed by experimental data in combination with hydrodynamic calculations, for Au-Au collisions at $\sqrt{s_{NN}} = 0.2$ TeV (left) [10] and Pb-Pb collisions at $\sqrt{s_{NN}} = 2.76$ TeV (right) [11] in various centrality windows (from top to bottom). Symbols are predictions from various models of initial conditions (see text for details).

flow for a given value of η/s, resulting in smaller values of ε_n. Although this result may seem natural, it is not trivial as it looks: the freeze-out temperature is adjusted so as to match the p_t spectrum, so that smaller t_0 goes along earlier freeze-out. Both effects essentially compensate each other at RHIC energies [8], so that final results were insensitive to t_0. The situation is different at LHC energies: in general, hydrodynamic results are less sensitive to the hadronic phase [68] and to the freeze-out temperature, which results in a stronger sensitivity of ε_n to initial flow.

In general, the takeaway message is that any effect that causes stronger collective flow tends to increase both ε_2 and ε_3 in such a way that the coefficient C in Eq. (5) is almost unchanged.

In fact, the largest contribution to the thickness of the uncertainty band comes not from properties of the medium or physical parameters, but instead from the linear-response approximation itself: weighting with entropy rather than energy yields slightly smaller values of ε_2, while ε_3 remains the same.

Once all sources of uncertainties are taken into account, one is left with an allowed region in the $(\varepsilon_2, \varepsilon_3)$ plane, corresponding to an allowed interval for the coefficient C in Eq. (5). The same procedure can be repeated for other centrality intervals, and at lower energy. The value $k = 0.6$ in Eq. (5) gives a good fit for all centralities at LHC, while $k = 0.5$ gives a better fit at RHIC. These allowed regions are displayed as shaded bands in Fig. 2. The uncertainty becomes larger as centrality percentile increases, which is mostly due to the difference between energy and entropy weighting. The minimum and maximum values of C are listed in Tables I and II for RHIC and LHC, respectively. In the same centrality range, the allowed band at LHC is slightly higher than at RHIC, but they overlap.

IV. TESTING INITIAL STATE MODELS

We now use the values of the rms ellipticity ε_2 and triangularity ε_3 obtained from data and hydrodynamic calculations as a filter for existing models of the initial state. Since ε_3 is solely created by fluctuations of the

TABLE I. Values of the ratio $\sqrt{\langle\varepsilon_2^2\rangle}/\sqrt{\langle\varepsilon_3^2\rangle}^{0.5}$ at RHIC. First two lines: minimum and maximum values allowed by hydrodynamics and experimental data. Next lines: values predicted by various models.

% centrality	0-10	10-20	20-30	30-40	40-50
minimum	0.36	0.56	0.69	0.75	0.74
maximum	0.41	0.63	0.79	0.90	0.91
MC-Glauber	0.38	0.57	0.69	0.76	0.80
MC-Glauber ($N_{\rm coll}$)	0.44	0.64	0.76	0.81	0.83
MC-Glauber ($N_{\rm part}$)	0.34	0.52	0.64	0.73	0.78
MC-KLN	0.49	0.78	0.95	1.03	1.06
MC-rcBK	0.49	0.73	0.87	0.95	0.98
IP-Glasma	0.43	-	0.76	0.85	-
DIPSY	0.39	0.59	0.72	0.80	0.84

TABLE II. Values of the ratio $\sqrt{\langle\varepsilon_2^2\rangle}/\sqrt{\langle\varepsilon_3^2\rangle}^{0.6}$ at LHC.

% centrality	0-5	5-10	10-20	20-30	30-40
minimum	0.40	0.58	0.76	0.88	0.94
maximum	0.43	0.65	0.87	1.06	1.13
MC-Glauber	0.39	0.50	0.66	0.78	0.85
MC-Glauber ($N_{\rm coll}$)	0.46	0.61	0.79	0.92	0.96
MC-Glauber ($N_{\rm part}$)	0.33	0.42	0.57	0.71	0.80
MC-KLN	0.46	0.73	0.98	1.17	1.25
MC-rcBK	0.48	0.67	0.88	1.04	1.12
IP-Glasma	0.43	-	0.83	0.97	1.03
DIPSY	0.40	0.58	0.76	0.90	0.95

initial geometry [6], in order to be consistent with data there is a trivial requirement that models take these fluctuations into account — typically these are Monte-Carlo models. The simplest is the Glauber model [69], where each participant nucleon adds a contribution to the initial density with Gaussian shape (in x and y) and width $\sigma = 0.4$ fm, a value commonly used in event-by-event hydrodynamic calculations [20, 70, 71]. We use the PHOBOS Monte-Carlo Glauber [72], though other implementations exist [73, 74]. Each participant can be given equal weight (referred to as "Glauber $N_{\rm part}$"), or a weight proportional to its number of collisions (referred to as "Glauber $N_{\rm coll}$" scaling), or a linear combination of the two, adjusted to match observed multiplicity spectra (default version, referred to simply as "Glauber") at RHIC [75] and LHC [76].

Another class of initial state models, which generically go under the name CGC, implement the idea of parton saturation [77]. They generally predict a larger ε_2 [56, 78]. In the earliest Monte-Carlo implementation [79], which we denote by MC-KLN, the source of fluctuations is essentially the same as in Glauber models, resulting in similar values of ε_3. Recent works tend to incorporate additional sources of fluctuations, at the subnucleonic level [80–83], resulting in general in larger ε_3. Specifically, we test the MC-rcBK model which incorporates negative binomial fluctuations in nucleon-nucleon collisions [82], the DIPSY model [81] which incorporates a BFKL gluon cascade, and the IP-Glasma model [83] which involves a classical Yang-Mills description of early-time gluon fields.

In all cases, centrality bins are assigned according to the total entropy of each Monte Carlo event, which corresponds closely to the total multiplicity that would be obtained after hydrodynamic evolution. Since the experimental centrality selection is also closely related to multiplicity, any systematics from centrality selection adds a negligible uncertainty and does not affect any of the following conclusions

Predictions of these initial-state models are plotted in Fig. 2, together with constrains from data and hydrodynamics. They are generally in the ballpark for all centralities. All models predict a strong increase of the rms ε_2 with centrality percentile (as the overlap area between colliding nuclei becomes more elongated) and a mild increase of the rms ε_3, driven by the decrease in the system size [84]. The evolution from RHIC to LHC at the same centrality depends on the model. The Glauber model predicts a decrease of both ε_2 and ε_3 by a few %, which is only partially explained by the increase in system size from Au to Pb. The MC-rcBK predicts similar values at RHIC and LHC. Finally, DIPSY predicts a mild increase of ε_2 while ε_3 is unchanged.

Eq. (5) provides a simple criterion for checking whether or not a particular model of initial conditions is compatible with data and hydrodynamics: one computes $\sqrt{\langle\varepsilon_2^2\rangle}/\sqrt{\langle\varepsilon_3^2\rangle}^k$ for this model, with $k = 0.5$ (0.6) at RHIC (LHC), and checks whether the result falls within the allowed band. This comparison is carried out in Tables I and II. One sees that the MC-KLN is excluded for all centralities at RHIC and LHC. It has already be noted that this particular model underpredicts v_3 at RHIC if tuned to reproduce v_2 [9, 10]. The MC-rcBK model is also excluded at RHIC, and marginally allowed at LHC. The Glauber model (in its default version with a superposition of number of participants and number of binary collisions) falls within the allowed band at RHIC, but is excluded at LHC, except for the most central bin. DIPSY and IP-Glasma fall within the allowed region for all centralities, and so does the Glauber model with pure binary collision scaling.

The statement of whether a particular model of initial conditions is compatible with data or not turns out to be quite robust with respect to several ambiguities in the definitions of ε_2 and ε_3. In the Glauber model, for instance, one treats each participant as a "source", whose width σ is a free parameter. There is also a similar ambiguity due to the unknown thermalization time: if one lets the system evolve for some time t_0 before evaluating ε_n, the values of ε_n depend on t_0. If one doubles

the value of σ, from 0.4 to 0.8 fm [20], ε_2 decreases by 6% and ε_3 decreases by 9% for central collision, but the ratios in Tables I and II only change by 2% and 1% respectively. This can be easily understood. It can be shown [84] that the smearing of the sources only affects the denominator of Eq. (1), while leaving the numerator unchanged: thus the only effect of source smearing is a small increase in the system size, resulting in smaller ε_n. Since $\{r^3\} \propto \{r^2\}^{2/3}$, ε_n decreases in such a way that the ratio $\varepsilon_2/(\varepsilon_3)^{2/3}$ remains constant. Comparing with Eq. (5), where k is close to 2/3, one sees that smearing results in a displacement of $(\varepsilon_2, \varepsilon_3)$ almost parallel to the allowed band: more or less smearing does not yield better or worse agreement with data.

V. CONCLUSIONS

Elliptic and triangular flow, v_2 and v_3, are determined by the ellipticity ε_2 and triangularity ε_3 of the initial density profile, and by the linear hydrodynamic response to these initial anisotropies. Experimental data on v_2 and v_3 thus allow to constrain the rms ε_2 and ε_3. By varying unknown parameters in the hydrodynamic calculations, we have obtained the corresponding uncertainties on the rms ε_2 and ε_3 at RHIC and LHC energies. They are strongly correlated, so that region allowed by data reduces in practice to a band in the (rms ε_2, rms ε_3) plane. We have described a simple test that can be performed on any candidate model of initial conditions to determine its compatibility with data.

While the main source of uncertainty in the hydrodynamic response is the viscosity over entropy ratio η/s, the uncertainty on the early stages is also significant. Both are correlated, in the sense that more initial flow can be compensated by a larger viscosity. For this reason, it is easier to constrain models of initial conditions than η/s.

We have shown that elliptic and triangular flow data can be used to exclude existing models of initial conditions. However, it is very difficult to constrain the granularity [85] of initial conditions from these data. As exemplified by Monte-Carlo Glauber simulations, changing the source size has a modest effect on ε_2 and ε_3. In addition, the resulting change has almost exactly the same effect as changing the viscosity, which is unknown. Therefore it is unlikely that the granularity can be constrained with just elliptic and triangular flow data as long as η/s is not precisely known. Other data can be used for this purpose, such as the detailed structure of 2-particle correlations [14].

The width of our error band is mostly due to the error on the linear response approximation itself, with the set of initial conditions that we have tested. Note that the deformation that we introduce to generate triangular flow, Eq. (4), is singular at the origin. With realistic initial conditions, one usually observes a stronger linear correlation between v_2 (v_3) and ε_2 (ε_3) then with our smooth initial conditions [19]. Repeating the calculation with realistic initial conditions could thus help reduce the width of the error band and yield tighter constraints on initial-state models.

ACKNOWLEDGMENTS

We thank the ALICE Collaboration for providing experimental data, and Jürgen Schukraft for helpful discussion. We also thank Christoffer Flensburg and Björn Schenke, for providing results from the DIPSY and IP-Glasma models. This work is funded by the European Research Council under the Advanced Investigator Grant ERC-AD-267258.

[1] S. A. Voloshin, A. M. Poskanzer and R. Snellings, arXiv:0809.2949 [nucl-ex].
[2] D. Teaney and L. Yan, Phys. Rev. C **83**, 064904 (2011).
[3] K. H. Ackermann *et al.* [STAR Collaboration], Phys. Rev. Lett. **86**, 402 (2001).
[4] K. Aamodt *et al.* [ALICE Collaboration], Phys. Rev. Lett. **105**, 252302 (2010) [arXiv:1011.3914 [nucl-ex]].
[5] J.-Y. Ollitrault, Phys. Rev. D **46**, 229 (1992).
[6] B. Alver and G. Roland, Phys. Rev. C **81**, 054905 (2010) [Erratum-ibid. C **82**, 039903 (2010)]
[7] P. Kovtun, D. T. Son and A. O. Starinets, Phys. Rev. Lett. **94**, 111601 (2005)
[8] M. Luzum and P. Romatschke, Phys. Rev. C **78**, 034915 (2008) [Erratum-ibid. C **79**, 039903 (2009)]
[9] B. H. Alver, C. Gombeaud, M. Luzum and J.-Y. Ollitrault, Phys. Rev. C **82**, 034913 (2010)
[10] A. Adare *et al.* [PHENIX Collaboration], Phys. Rev. Lett. **107**, 252301 (2011)
[11] K. Aamodt *et al.* [ALICE Collaboration], Phys. Rev. Lett. **107**, 032301 (2011)
[12] N. Borghini, P. M. Dinh and J.-Y. Ollitrault, Phys. Rev. C **63**, 054906 (2001)
[13] R. P. G. Andrade, F. Grassi, Y. Hama, T. Kodama and W. L. Qian, Phys. Rev. Lett. **101**, 112301 (2008)
[14] F. G. Gardim, F. Grassi, M. Luzum and J.-Y. Ollitrault, Phys. Rev. C **87**, 031901 (2013)
[15] N. Borghini and J.-Y. Ollitrault, Phys. Lett. B **642**, 227 (2006)
[16] P. Bozek, Phys. Rev. C **81**, 034909 (2010)
[17] U. W. Heinz and R. Snellings, Annu. Rev. Nucl. Part. Sci. **63**, 123 (2013)
[18] G. Aad *et al.* [ATLAS Collaboration], Phys. Rev. C **86**, 014907 (2012)
[19] H. Niemi, G. S. Denicol, H. Holopainen and P. Huovinen, Phys. Rev. C **87**, 054901 (2013)
[20] H. Holopainen, H. Niemi and K. J. Eskola, Phys. Rev. C **83**, 034901 (2011)
[21] B. Alver *et al.* [PHOBOS Collaboration], Phys. Rev. Lett. **98**, 242302 (2007)
[22] H. Petersen, G. -Y. Qin, S. A. Bass and B. Muller, Phys.

Rev. C **82**, 041901 (2010)
[23] R. S. Bhalerao, M. Luzum and J.-Y. Ollitrault, Phys. Rev. C **84**, 034910 (2011)
[24] F. G. Gardim, F. Grassi, Y. Hama, M. Luzum and J.-Y. Ollitrault, Phys. Rev. C **83**, 064901 (2011)
[25] E. Retinskaya, M. Luzum and J.-Y. Ollitrault, Phys. Rev. Lett. **108**, 252302 (2012)
[26] F. G. Gardim, F. Grassi, M. Luzum and J.-Y. Ollitrault, Phys. Rev. C **85**, 024908 (2012)
[27] D. Teaney and L. Yan, Phys. Rev. C **86**, 044908 (2012)
[28] D. Teaney and L. Yan, Nucl. Phys. A904-905 **2013**, 365c (2013)
[29] M. Miller and R. Snellings, nucl-ex/0312008.
[30] B. Alver, B. B. Back, M. D. Baker, M. Ballintijn, D. S. Barton, R. R. Betts, R. Bindel and W. Busza *et al.*, Phys. Rev. C **77**, 014906 (2008)
[31] S. Afanasiev *et al.* [PHENIX Collaboration], Phys. Rev. C **80**, 024909 (2009)
[32] C. Gale, S. Jeon and B. Schenke, Int. J. Mod. Phys. A **28**, 1340011 (2013).
[33] M. Luzum and J.-Y. Ollitrault, Nucl. Phys. A904-905 **2013**, 377c (2013)
[34] R. A. Soltz, I. Garishvili, M. Cheng, B. Abelev, A. Glenn, J. Newby, L. A. Linden Levy and S. Pratt, Phys. Rev. C **87**, 044901 (2013)
[35] J. D. Bjorken, Phys. Rev. D **27**, 140 (1983).
[36] S. Chatrchyan *et al.* [CMS Collaboration], Eur. Phys. J. C **72**, 2012 (2012)
[37] L. Adamczyk *et al.* [STAR Collaboration], Phys. Rev. C 88, **014904** (2013)
[38] M. Luzum and P. Romatschke, Phys. Rev. Lett. **103**, 262302 (2009)
[39] M. Luzum, Phys. Rev. C **83**, 044911 (2011)
[40] Z. Qiu and U. W. Heinz, Phys. Rev. C **84**, 024911 (2011)
[41] T. Epelbaum and F. Gelis, Phys. Rev. Lett. **111**, 232301 (2013)
[42] P. F. Kolb and U. W. Heinz, In *Hwa, R.C. (ed.) et al.: Quark gluon plasma* 634-714
[43] M. Gyulassy, Y. .M. Sinyukov, I. .Karpenko and A. V. Nazarenko, Braz. J. Phys. **37**, 1031 (2007).
[44] W. Broniowski, M. Chojnacki, W. Florkowski and A. Kisiel, Phys. Rev. Lett. **101**, 022301 (2008)
[45] S. Pratt, Phys. Rev. Lett. **102**, 232301 (2009)
[46] J. Vredevoogd and S. Pratt, Phys. Rev. C **79**, 044915 (2009)
[47] J.-Y. Ollitrault, Eur. J. Phys. **29**, 275 (2008)
[48] H. B. Meyer, Phys. Rev. D **76**, 101701 (2007)
[49] H. Song, Nucl. Phys. A904-905 **2013**, 114c (2013)
[50] K. Dusling and D. Teaney, Phys. Rev. C **77**, 034905 (2008)
[51] G. S. Denicol, T. Kodama, T. Koide and P. .Mota, Phys. Rev. C **80**, 064901 (2009)
[52] K. Dusling and T. Schäfer, Phys. Rev. C **85**, 044909 (2012)
[53] F. Karsch, D. Kharzeev and K. Tuchin, Phys. Lett. B **663**, 217 (2008)
[54] R. Baier, P. Romatschke, D. T. Son, A. O. Starinets and M. A. Stephanov, JHEP **0804**, 100 (2008)
[55] D. Teaney, J. Lauret and E. V. Shuryak, Phys. Rev. Lett. **86**, 4783 (2001)
[56] T. Hirano, U. W. Heinz, D. Kharzeev, R. Lacey and Y. Nara, Phys. Lett. B **636**, 299 (2006)
[57] H. Song, S. A. Bass and U. Heinz, Phys. Rev. C **83**, 054912 (2011) [Erratum-ibid. C **87**, 019902 (2013)]
[58] T. Hirano, P. Huovinen, K. Murase and Y. Nara, Prog. Part. Nucl. Phys. **70**, 108 (2013)
[59] S. Ryu, S. Jeon, C. Gale, B. Schenke and C. Young, Nucl. Phys. A904-905 **2013**, 389c (2013)
[60] A. Monnai and T. Hirano, Phys. Rev. C **80**, 054906 (2009)
[61] P. Bozek and I. Wyskiel-Piekarska, Phys. Rev. C **85**, 064915 (2012)
[62] D. Teaney, Phys. Rev. C **68**, 034913 (2003)
[63] D. Teaney and L. Yan, arXiv:1304.3753 [nucl-th].
[64] K. Dusling, G. D. Moore and D. Teaney, Phys. Rev. C **81**, 034907 (2010)
[65] M. Luzum and J.-Y. Ollitrault, Phys. Rev. C **82**, 014906 (2010)
[66] P. F. Kolb, Heavy Ion Phys. **15**, 279 (2002)
[67] M. Luzum, Phys. Lett. B **696**, 499 (2011)
[68] H. Niemi, G. S. Denicol, P. Huovinen, E. Molnar and D. H. Rischke, Phys. Rev. C **86**, 014909 (2012)
[69] M. L. Miller, K. Reygers, S. J. Sanders and P. Steinberg, Ann. Rev. Nucl. Part. Sci. **57**, 205 (2007)
[70] B. Schenke, S. Jeon and C. Gale, Phys. Rev. Lett. **106**, 042301 (2011)
[71] P. Bozek and W. Broniowski, Phys. Lett. B **718**, 1557 (2013)
[72] B. Alver, M. Baker, C. Loizides and P. Steinberg, arXiv:0805.4411 [nucl-ex].
[73] W. Broniowski, M. Rybczynski and P. Bozek, Comput. Phys. Commun. **180**, 69 (2009)
[74] M. Rybczynski, G. Stefanek, W. Broniowski and P. Bozek, arXiv:1310.5475 [nucl-th].
[75] S. S. Adler *et al.* [PHENIX Collaboration], Phys. Rev. C **71**, 034908 (2005) [Erratum-ibid. C **71**, 049901 (2005)]
[76] B. Abelev *et al.* [ALICE Collaboration], Phys. Rev. C **88**, 044909 (2013)
[77] D. Kharzeev and M. Nardi, Phys. Lett. B **507**, 121 (2001)
[78] T. Lappi and R. Venugopalan, Phys. Rev. C **74**, 054905 (2006)
[79] H.-J. Drescher and Y. Nara, Phys. Rev. C **76**, 041903 (2007)
[80] J. L. Albacete and A. Dumitru, arXiv:1011.5161 [hep-ph].
[81] C. Flensburg, arXiv:1108.4862 [nucl-th].
[82] A. Dumitru and Y. Nara, Phys. Rev. C **85**, 034907 (2012)
[83] B. Schenke, P. Tribedy and R. Venugopalan, Phys. Rev. C **86**, 034908 (2012)
[84] R. S. Bhalerao, M. Luzum and J.-Y. Ollitrault, Phys. Rev. C **84**, 054901 (2011)
[85] H. Petersen, C. Coleman-Smith, S. A. Bass and R. Wolpert, J. Phys. G **38**, 045102 (2011)